International Journal of Minerals, Metallurgy and Materials
Volume 23, Number 7, July 2016, Page 743
DOI: 10.1007/s12613-016-1288-y

Removal of phosphorus-rich phase from high-phosphorous iron ore by melt separation at 1573 K in a super-gravity field

Jin-tao Gao, Lei Guo, Yi-wei Zhong, Hong-ru Ren, and Zhan-cheng Guo

State Key Laboratory of Advanced Metallurgy, University of Science and Technology Beijing, Beijing 100083, China
(Received: 25 December 2015; revised: 4 March 2016; accepted: 7 March 2016)

Abstract: A new approach of removing the phosphorus-rich phase from high-phosphorous iron ore by melt separation at 1573 K in a super-gravity field was investigated. The iron–slag separation by super-gravity resulted in phosphorus being effectively removed from the iron-rich phase and concentrated as a phosphorus-rich phase at a temperature below the melting point of iron. The samples obtained by super-gravity exhibited obvious layered structures. All the iron grains concentrated at the bottom of the sample along the super-gravity direction, whereas the molten slag concentrated in the upper part of the sample along the opposite direction. Meanwhile, fine apatite crystals collided and grew into larger crystals and concentrated at the slag–iron interface. Consequently, in the case of centrifugation with a gravity coefficient of $G = 900$, the mass fractions of the slag phase and iron-rich phase were similar to their respective theoretical values. The mass fraction of MFe in the iron-rich phase was as high as 97.77wt% and that of P was decreased to 0.092wt%.

Keywords: ironmaking; super-gravity; melt separation; dephosphoration

1. Introduction

With the rapid consumption of iron ore resources, the remaining iron ore deposits exhibit an increasing complex mineralogical composition. Therefore, the development of methods to exploit refractory iron ores has become urgent. For example, high-phosphorous iron ore resources are available in massive reserves but cannot be used on a large scale for blast-furnace iron making because of their high phosphorous content [1−2]. Furthermore, the apatite and hematite phases with minor differences in density and magnetic properties are intimately intermixed in high-phosphorous iron ore; thus, grinding the ore into a sufficiently fine size for the iron oxides to be directly separated from the phosphorus-containing phases by conventional beneficiation methods is not practical [3−4]. We previously ground high-phosphorous iron ore to ultrafine 0.01–0.001 mm particles using a jet mill, which led to the dissociation of apatite and hematite phases; however, the phosphorus-rich and iron-rich phases were not effectively separated from the ultrafine reduced ore by magnetic separation [5]. Thus far, many hydrometallurgy methods [6–7] and pyrometallurgy methods have been proposed to deal with such refractory iron ore.

The proposed pyrometallurgy methods mainly include the coal- and gas-based direct reduction processes [8−9]. Compared with coal-based direct reduction, the iron oxide phase can be reduced by H_2/CO at a temperature lower than 1273 K, whereas the apatite phase is difficult to reduce in this temperature range. Therefore, Zhao *et al.* [10] studied the gas-based reduction of high-phosphorous iron ore powders by H_2/CO in a tube furnace at 1073–1273 K, and Guo *et al.* [11] investigated the same process in a fluidized bed. They both reported that the iron oxide could be reduced by H_2/CO at temperatures lower than 1273 K and with a high extent of reduction, whereas the phosphorus remained in the apatite phase. Tang *et al.* [12] studied the gas-based reduction of the ore after a microwave treatment, and their results showed that the oolitic component of high-phosphorous iron ore generated cracks and fissures under microwave irradiation, which facilitated the gas-based reduction process. However, gas-based direct reduction carried out at lower

Corresponding author: Zhan-cheng Guo E-mail: zcguo@ustb.edu.cn

temperatures is always combined with a high-temperature melt separation process to further separate molten metal and slag. Guo *et al.* [11] studied the melt separation of hydrogen-reduced ore by adding sufficient CaO to bring the slag basicity to 1.5 at 1823 K, which resulted in the effective separation of molten metal and slag; however, the phosphorous content of the metal was as high as 0.82wt%. Tang *et al.* [12] further investigated the melt separation of gaseous-reduced ore after microwave treatment by adding CaO and Na_2CO_3 at 1823–1873 K; in this case, the phosphorous content in the metal was decreased to 0.31wt%.

With respect to the transform mechanism of phosphorus between the metal and slag phases during the melt separation process when no carbon is present in the reduced ore, Zhao *et al.* [10] and Tang *et al.* [12] considered that the phosphorus existed in the metal as apatite inclusions, whereas Guo *et al.* [11] inferred that the phosphorus was smelted into the metal via the reactions between Fe and P_2O_5. Hamano *et al.* [13−14] has extensively studied the reaction mechanism of $2CaO{\cdot}SiO_2$ and FeO_x–CaO–SiO_2–P_2O_5 slag at 1573 K and reported different mass transfer characteristics of phosphorus between the $2CaO{\cdot}SiO_2$ particles and the molten slag. Consequently, reducing the iron–slag separation temperature to 1573 K, which is below the melting point of iron, would not only be beneficial for keeping the phosphorus out of the iron-rich phase but also for concentrating the phosphorus-rich phase.

Given that the super-gravity technology has been successfully applied in removing impurities from alloy melts [15−16], we here conducted melt-separation experiments on iron-rich, slag, and phosphorus-rich phases from reduced high-phosphorous iron ore at 1573 K in a super-gravity field. The influences of the super-gravity field on the microstructures, mineral compositions, and components of the iron-rich, slag, and phosphorus-rich phases were also investigated.

2. Experimental

2.1. Material

High-phosphorous iron ore from Hubei Province of China was used as the raw material in this study. The ore's chemical composition is listed in Table 1, and the mass fractions of total iron (TFe) and phosphorus (P) are 50.15wt% and 0.81wt%, respectively. The mineral phases, which were characterized by X-ray diffraction (XRD), mainly include hematite, quartz, and apatite, as shown in Fig. 1, and the phosphorus exists in the form of apatite.

Table 1. Chemical compositions of the high-phosphorous iron ore before and after gaseous reduction wt%

Composition	TFe	FeO	MFe	SiO_2	CaO	Al_2O_3	MgO	P
Iron ore	50.15	1.56	—	13.15	4.80	4.52	0.48	0.81
Reduced ore with basicity of 1.0	58.20	14.97	46.55	15.25	15.25	5.25	0.56	0.94

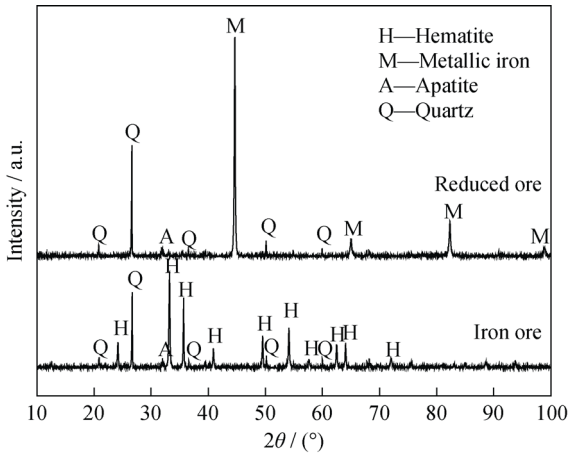

Fig. 1. XRD patterns of the high-phosphorous iron ore before and after gaseous reduction.

The lump ore was crushed and screened to powders with particle sizes ranging from 0.90 to 0.11 mm, and the resulting powders were reduced in a fluidized bed [17] under an Ar and H_2 atmosphere at 1073 K for 120 min. The variations in the mineralogical compositions before and after gaseous reduction (Fig. 1) revealed that only the hematite was reduced into metallic iron; the phosphorus was still in the form of apatite after gaseous reduction.

2.2. Apparatus

The super-gravity field used in melt-separation experiments of the reduced high-phosphorous iron ore was generated by a centrifugal apparatus; its schematic is illustrated in Fig. 2. The heating furnace and a counterweight were fixed symmetrically to the centrifugal rotor to maintain verticality in the stationary state and to change into a level state when the centrifugal rotor was running. Moreover, the heating furnace was heated by the resistance wire, and the temperature was controlled by a program controller with an R-type thermocouple.

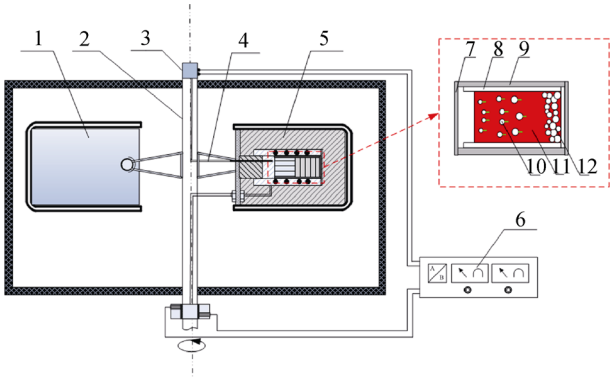

Fig. 2. Schematic of the centrifugal apparatus: 1. counterweight; 2. centrifugal axis; 3. conductive slipping; 4. thermocouple; 5. insulating layer; 6. temperature controller; 7. graphite lid; 8. alumina crucible; 9. graphite crucible; 10. iron grains; 11. slag phase; 12. iron-rich phase.

2.3. Experimental and analytical procedures

To achieve a lower melting temperature of the slag phase, the slag basicity, defined as the CaO/SiO_2 mass ratio, was adjusted from 0.37 to 1.00 by adding CaO to the reduced ore in quantities calculated on the basis of the experimental results reported by Guo *et al.* [11] and Tang *et al.* [12]. 10 g of reduced ore was placed into a high-purity alumina crucible with an inner diameter of 12 mm, and this crucible was placed into a graphite crucible with an inner diameter of 19 mm and covered with a graphite lid. The crucibles were then heated to 1573 K in the heating furnace of the centrifugal apparatus. The centrifugal apparatus was started and adjusted to an angular velocity of 1036, 1465, or 1794 r/min, corresponding to $G = 300$, $G = 600$, or $G = 900$, respectively, at a constant temperature of 1573 K for 10 min. Afterwards, the centrifugal apparatus was shut off and the graphite crucible was removed and water-quenched. The gravity coefficient (G) was defined as the ratio of super-gravitational acceleration to the normal gravitational acceleration via the following equation:

$$G = \frac{\sqrt{g^2 + (\omega^2 R)^2}}{g} = \frac{\sqrt{g^2 + \left(\frac{N^2 \pi^2 R}{900}\right)^2}}{g} \quad (1)$$

where G is the gravity coefficient, g is the normal gravitational acceleration ($g = 9.80$ m/s^2), w is the angular velocity (rad·s^{-1}), N is the rotating speed of the centrifugal apparatus (r/min), and R is the distance from the centrifugal axis to the center of the sample ($R = 0.25$ m). Simultaneously, a parallel experiment was carried out at 1573 K for 10 min without centrifugal treatment.

The samples obtained by experiments were sectioned longitudinally along the center axis, which was along the direction of super-gravity. One sample section was characterized by scanning electron microscopy-energy dispersive X-ray spectroscopy (SEM-EDS) to analyze the microstructures of the iron-rich and slag phases as well as the distribution and mineral composition of the phosphorus-rich phase in different areas of the sample. This sample section was then further characterized by metallographic microscopy and image analysis using the line intercept method to observe the variations in volume fraction and equivalent diameter of the slag inclusion in different areas of the iron-rich phase. The slag phase was crushed and divided from the iron-rich phase in another sample section along the interface between these phases, and the mass fractions of the slag and iron-rich phases were calculated by measuring their respective mass. The mass fractions of metallic iron (MFe) in the iron-rich phases were then measured by the chemical analytical method according to GB 6730.6—86, and those of phosphorus were measured by the inductively coupled plasma (ICP) method with an OPTIMA 7000DV.

3. Results and discussion

3.1. Macrostructure and microstructure of the sample obtained by super-gravity

The vertical profiles of the samples obtained by super-gravity with gravity coefficients of $G = 300$, $G = 600$, and $G = 900$ compared with the parallel sample are shown in Fig. 3. In a macroscopic view, layered structures were

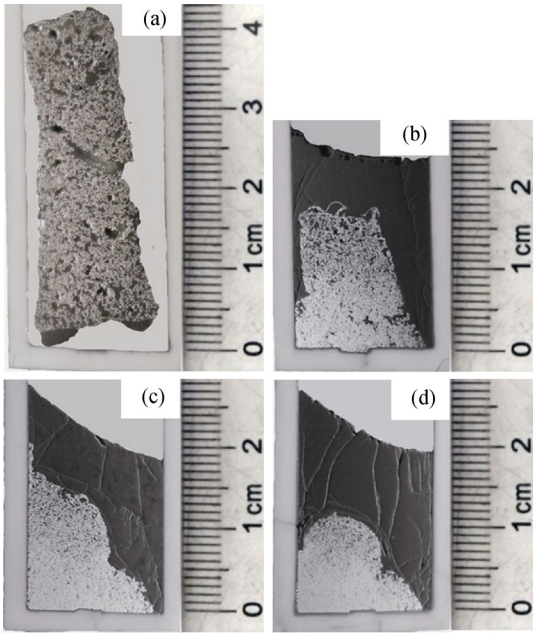

Fig. 3. Vertical profiles of the samples obtained by super-gravity compared with the parallel sample: (a) $G = 1$, (b) $G = 300$, (c) $G = 600$, and (d) $G = 900$.

apparent in the sample obtained by super-gravity, where the upper area of the sample was in a black glassy state and the bottom area was in a bright-white metal state. By contrast, the sample obtained in the absence of super-gravity exhibited a homogeneous structure.

SEM analysis results for the microstructures and EDS spectra of different areas in the layered sample obtained by super-gravity with a gravity coefficient of G = 900 are shown in Fig. 4. The bottom area was obviously an iron-rich phase, and the upper area was the slag phase. In a microscopic view, the iron-rich phase exhibited a porous structure with some fine slag included. The slag phase exhibited a compact structure in which iron grains were not observed. All the iron grains apparently moved to the bottom of the sample along the direction of super-gravity because of the greater density of iron compared to the densities of the other minerals and then concentrated as an iron-rich phase. The other minerals formed a molten slag, moved to the upper part of the sample along the direction opposite super-gravity, and then concentrated as a slag phase.

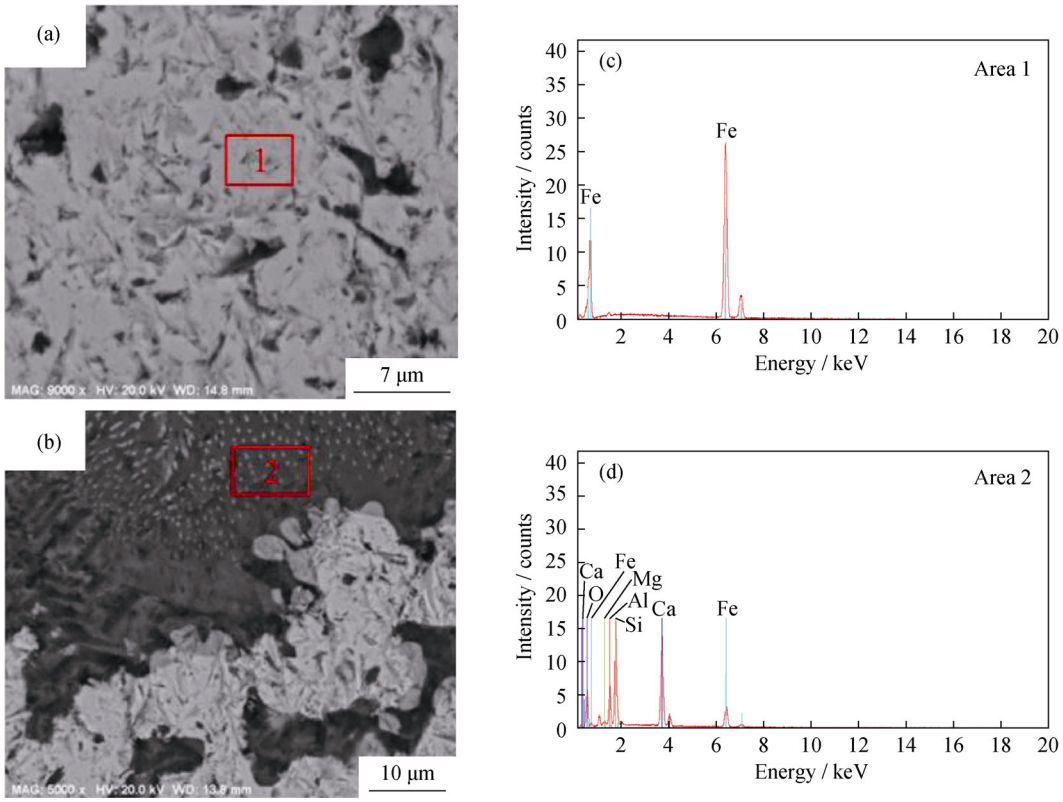

Fig. 4. SEM images and EDS spectra of different areas of the layered sample obtained by super-gravity with G = 900: (a) SEM image of the iron-rich phase, (b) SEM image of the slag phase, (c) EDS spectrum of the iron-rich phase, and (d) EDS spectrum of the slag phase.

3.2. Volume fraction and equivalent diameter of the slag inclusions in the iron-rich phase

To further investigate the microstructure of the iron-rich phase in the layered sample, the iron-rich phases were divided into four areas along the super-gravity direction and characterized by metallographic microscopy, as shown in Fig. 5. The enrichment degree of iron grains was substantially greater in the area approaching the bottom of the sample along the direction of super-gravity. The variations of volume fractions and equivalent diameters of the slag inclusions in different areas of the iron-rich phases with different gravity coefficients (Fig. 6) reveal that both the volume fraction and equivalent diameter of slag inclusions gradually decreased from the upper area (D) to the bottom area (A). These variations also reveal that the minimum values both occurred in the bottom area (A), where the iron grains concentrated into a compact iron-joined crystal. This observation is further evidenced that the iron grains moved, collided, and concentrated along the super-gravity direction, whereas the molten slag moved in the opposite direction and separated from the iron-rich phase, with a small amount included in the upper area of the iron-rich phase. Consequently, both the volume fraction and equivalent diameter of the slag inclusion in the iron-rich phase decreased substantially as the gravity coefficient was increased from G = 300 to G = 900.

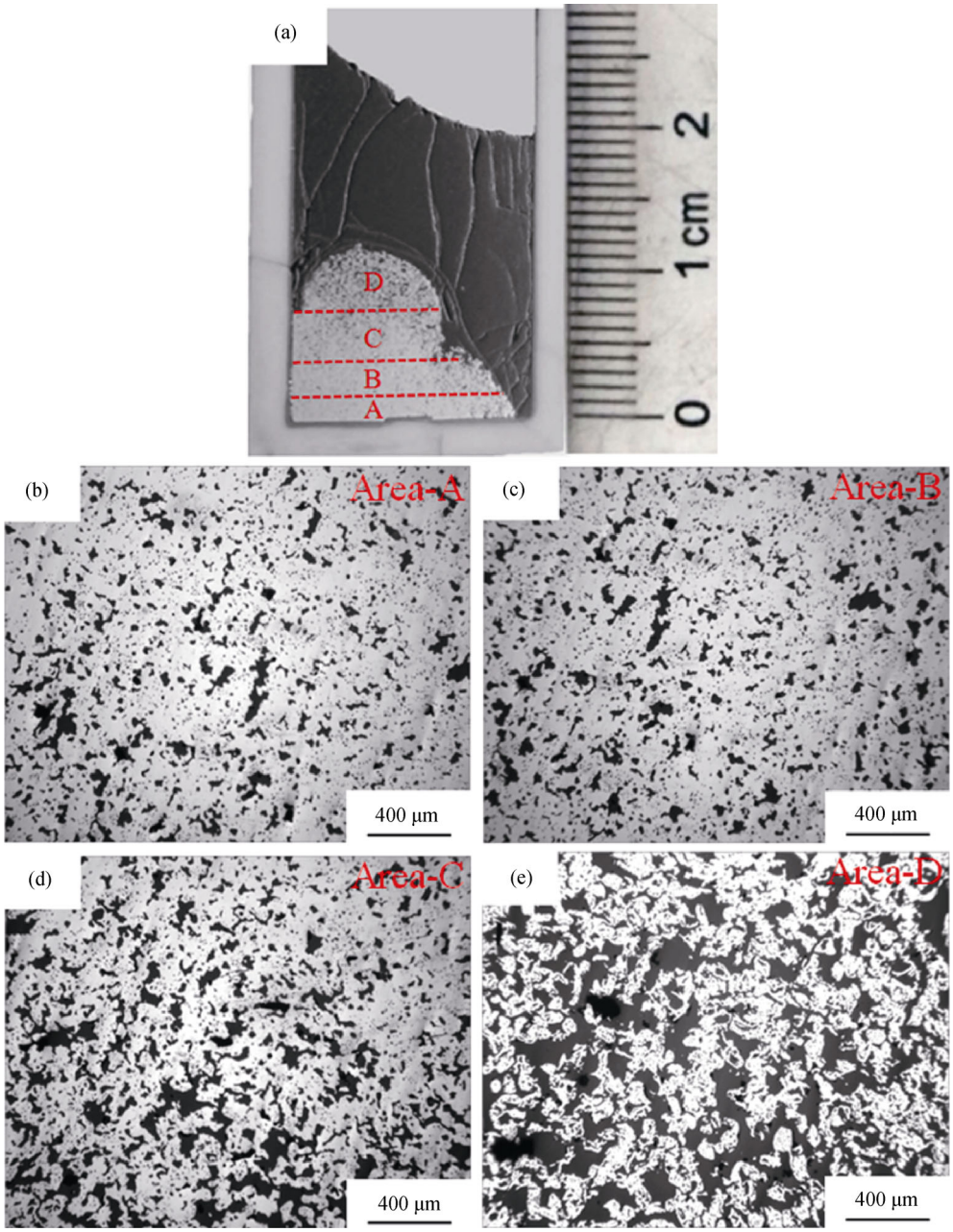

Fig. 5. Micrographs of different areas in the iron-rich phase obtained by super-gravity with G = 900: (a) positions of four areas in the layered sample and (b)–(e) micrographs of these four areas in the iron-rich phase.

3.3. Distribution of the phosphorus-rich phase in the layered sample

The SEM-EDS mapping of the phosphorus-rich phase in different areas of the layered sample obtained by super-gravity with a gravity coefficient of G = 900 is shown in Figs. 7 and 8. Most of the phosphorus-rich phase was concentrated at the slag–iron interface, and a small amount was contained in the slag inclusion in the upper iron-rich phase. Moreover, these phosphorus-rich phases were mainly in the form of larger equiaxed crystals and columnar crystals with sizes ranging from 0.02 to 0.08 mm. These results, combined with EDS data given in Table 2, indicated that these phosphorus-rich phases were mainly composed of calcium (38.82wt%–40.03wt%), phosphorus (18.26wt%–19.33wt%), oxygen (37.89wt%–40.00wt%), and a small amount of silicon (0.58wt%–2.59wt%). The phosphorus still existed in the form of apatite and the fine apatite crystals moved along the opposite direction of super-gravity, collided with each other, and grew into larger equiaxed crystals or columnar crystals.

Most of the larger apatite crystals thereafter concentrated in the slag–iron interface because the density of this region was intermediate between those of the slag and the iron-rich phase [14−15]; however, a few apatite crystals were intercepted and stopped in the slag inclusion in the upper area of the iron-rich phase.

3.4. Components of the slag and iron-rich phases after super-gravity treatment

The mass fractions of the slag and iron-rich phases obtained by super-gravity with different gravity coefficients are shown in Table 3. The super-gravity field was beneficial for the separation of the slag phase and iron-rich phase, and an increase in the gravity coefficient effectively increased its separation effect. Consequently, in the case of a gravity coefficient of G = 900, the mass fractions of the slag phase and iron-rich phase were 52.65% and 47.35%, respectively, which are similar to their respective theoretical values. Measured by the chemical analytical method, the mass fractions of MFe in the iron-rich phases with different gravity coefficients are shown in Fig. 9. Increasing the gravity coefficient from G = 1 to G = 900 enhanced the

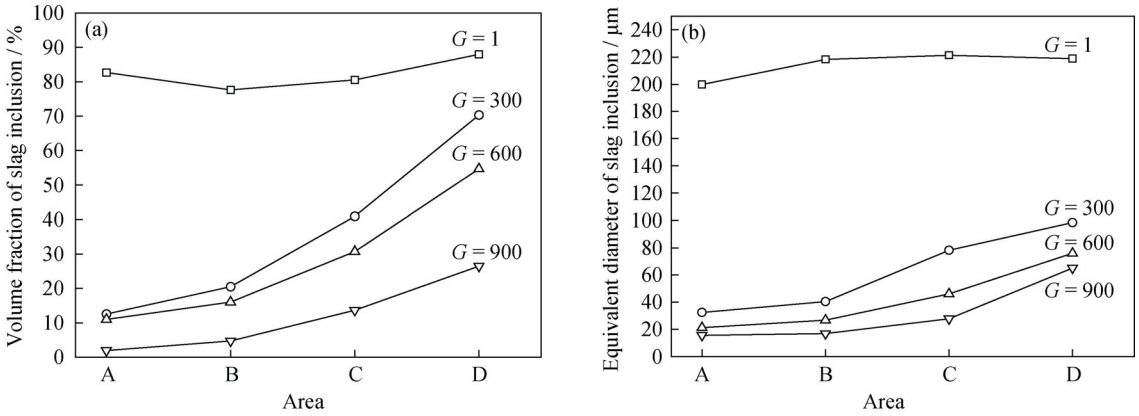

Fig. 6. Variations in volume fraction (a) and equivalent diameter (b) of the slag inclusion in different areas of the iron-rich phases.

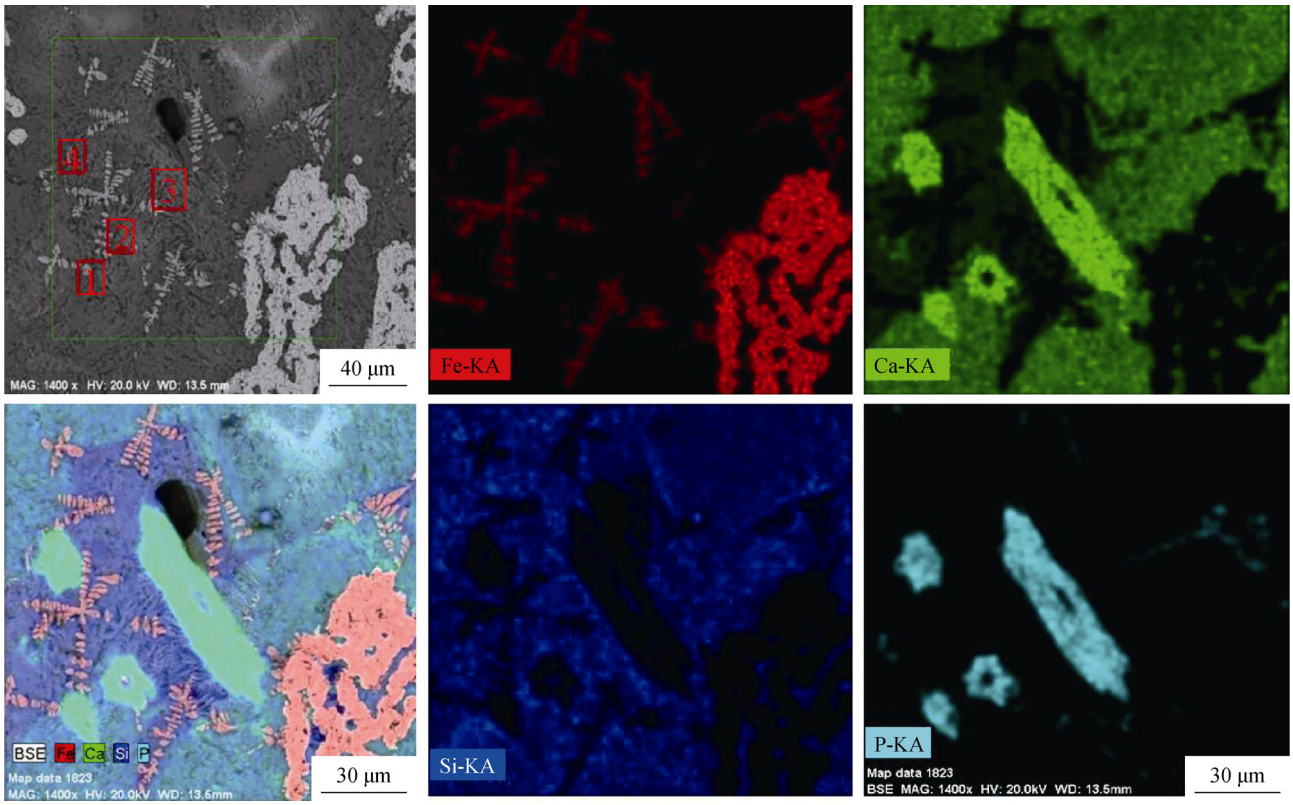

Fig. 7. SEM-EDS mapping of the phosphorus-rich phase in the slag–iron interface of the layered sample obtained by super-gravity with G = 900.

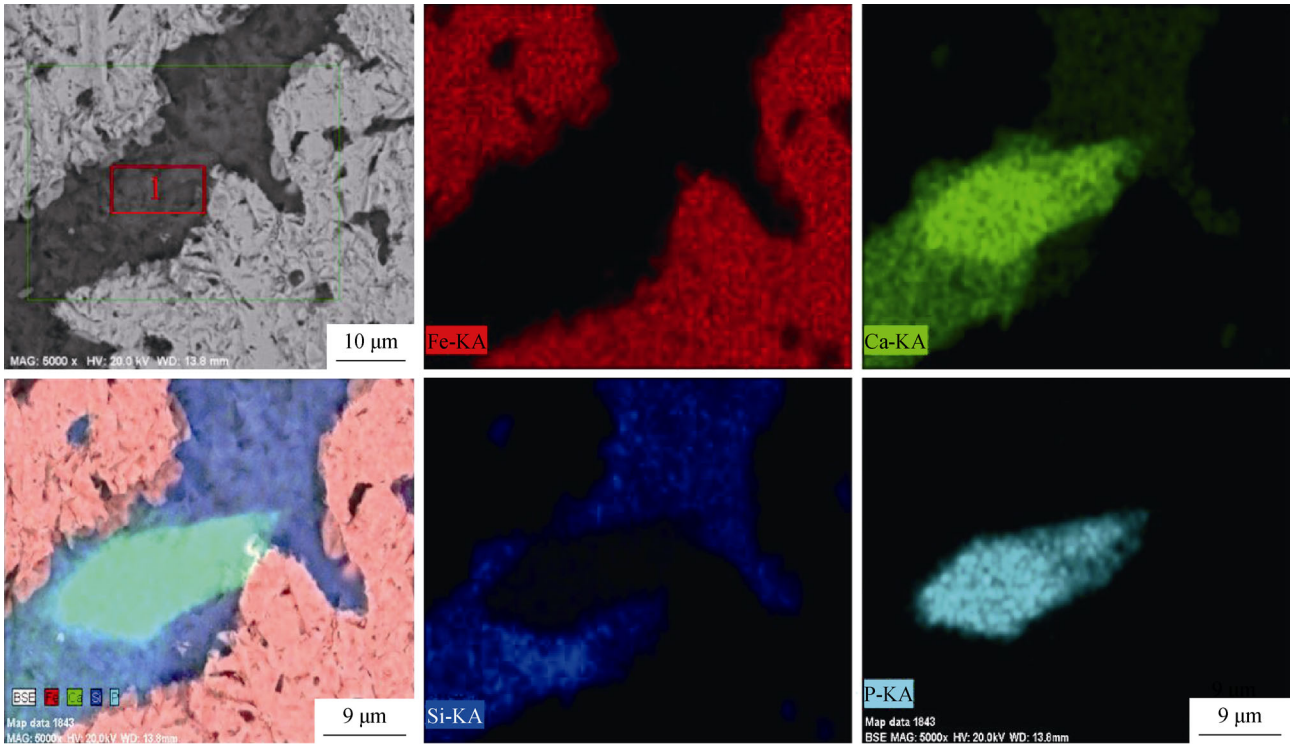

Fig. 8. SEM-EDS mapping of the phosphorus-rich phase in the upper area of the iron-rich phase of the layered sample obtained by super-gravity with G = 900.

Table 2. EDS data of the phosphorus-rich phases in different areas of the layered sample obtained by super-gravity with G = 900 wt%

Position	Area	Ca	P	O	Si	Fe
In the slag–iron interface	Fig. 7: 1	40.03	18.65	38.73	2.59	—
	Fig. 7: 2	39.50	19.17	39.39	1.94	—
	Fig. 7: 3	38.82	19.33	40.00	1.85	—
	Fig. 7: 4	39.92	19.04	37.89	0.58	2.57
In the upper area of iron-rich phase	Fig. 8: 1	39.23	18.26	38.02	1.05	3.44

Table 3. Mass fractions of the slag and iron-rich phases obtained by super-gravity with different gravity coefficients %

Samples	Gravity coefficient				Theoretical values
	1	300	600	900	
Slag phase	3.12	38.86	42.38	52.65	53.45
Iron-rich phase	96.88	61.14	57.62	47.35	46.55

content of MFe in the iron-rich phase from 47.68wt% to 97.77wt%.

Simultaneously, the mass fractions of phosphorus in the iron-rich phases with different gravity coefficient were measured by the ICP method; the results are shown as the solid line in Fig. 10. The mass fraction of phosphorus in the iron-rich phase decreased substantially, from 0.960wt% to 0.174wt%, when the gravity coefficient was increased from G = 1 to G = 900. Given that the residual phosphorus in the iron-rich phase may be caused by the slag inclusion, the iron-rich phases were further finely ground and magnetically separated to remove the visible slag inclusion. The mass fractions of phosphorous were then measured again; the results are shown as the dashed line in Fig. 10. The results clearly demonstrate that the mass fraction of phosphorus can be further decreased to 0.092wt% after removing the slag inclusion from the iron-rich phase with gravity coefficient of G = 900.

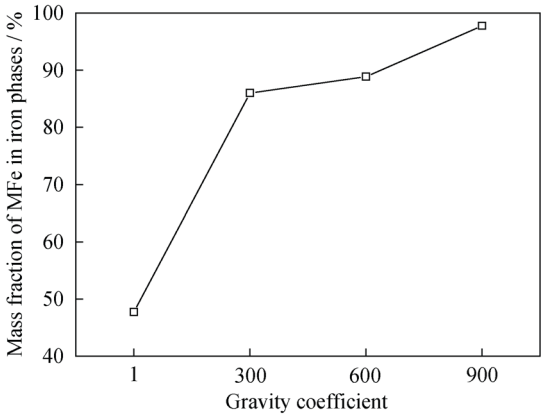

Fig. 9. Mass fractions of MFe in the iron-rich phases obtained by super-gravity with different gravity coefficients.

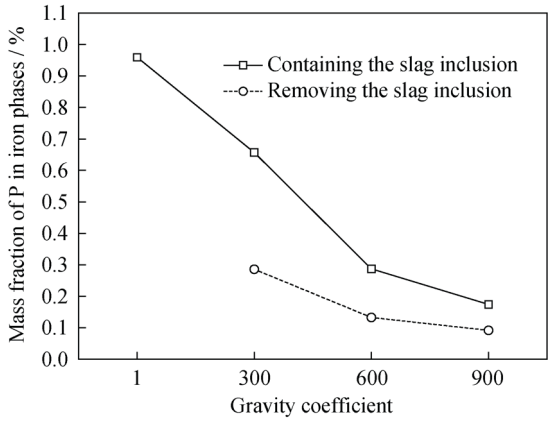

Fig. 10. Mass fractions of phosphorus in the iron-rich phases obtained by super-gravity with different gravity coefficients.

4. Conclusions

Through this experimental study, phosphorus was effectively removed from high-phosphorous iron ore by melt-separation at a low temperature of 1573 K in a super-gravity field. The following conclusions were drawn:

(1) The samples obtained by super-gravity exhibited layered structures. The iron grains concentrated at the bottom of the sample along the super-gravity direction, whereas the molten slag concentrated at the upper part of the sample along the opposite direction; apatite crystals concentrated in the slag–iron interface.

(2) In the case of a gravity coefficient of G = 900, the mass fractions of the slag phase and iron-rich phase were 52.65wt% and 47.35wt%, which are similar to their theoretical values, respectively. Meanwhile, the mass fraction of MFe in the iron-rich phase was 97.77wt%, whereas the mass fraction of phosphorus was decreased to 0.092wt%.

Acknowledgements

This work was financially supported by the National Natural Science Foundations of China (Nos. 51404025 and 51234001) and the Fundamental Research Funds for the Central Universities of China (FRF-TP-15-009A2).

References

[1] J. Diao, X. Liu, T. Zhang, and B. Xie, Mass transfer of phosphorus in high-phosphorus hot-metal refining, *Int. J. Miner. Metall. Mater.*, 22(2015), No. 3, p. 249.

[2] J. Wu, Z.J. Wen, and M.J. Cen, Development of technologies for high phosphorus oolitic hematite utilization, *Steel Res. Int*., 82(2011), No. 5, p. 494.

[3] R.C. Guimarães, A.C. Araugo, and A.E.C. Peres, Reagents in igneous phosphate ores flotation, *Miner. Eng*., 18(2005), No. 2, p. 199.

[4] A.P.L. Nunes, C.L.L. Pinto, G.E.S. Valadão, and P.R.M. Viana, Floatability studies of wavellite and preliminary results on phosphorus removal from a Brazilian iron ore by froth flotation, *Miner. Eng*., 39(2012), p. 206.

[5] J.T. Gao, L. Guo, and Z.C. Guo, Separation of P phase and Fe phase in high phosphorus oolitic iron ore by ultrafine grinding and gaseous reduction in a rotary furnace, *Metall. Mater. Trans. B*, 46(2015), No. 15, p. 2180.

[6] J.T. Yu, Z.C. Guo, and H.Q. Tang, Dephosphorization treatment of high phosphorus oolitic iron ore by hydrometallurgical process and leaching kinetics, *ISIJ Int*., 53(2013), No. 12, p. 2056.

[7] M.J. Fisher-White, R.R. Lovel, and G.J. Sparrow, Phosphorus removal from goethitic iron ore with a low temperature heat treatment and a caustic leach, *ISIJ Int*., 52(2012), No. 5, p. 797.

[8] W. Yu, T.C. Sun, J. Kou, Y.X. Wei, C.Y. Xu, and Z.Z. Liu, The function of $Ca(OH)_2$ and Na_2CO_3 as additive on the reduction of high-phosphorus oolitic hematite–coal mixed pellets, *ISIJ Int*., 53(2013), No. 3, p. 427.

[9] S.J. Bai, S.M. Wen, D.W. Liu, W.D. Zhang, and Y.J. Xian, Catalyzing carbothermic reduction of siderite ore with high content of phosphorus by adding sodium carbonate, *ISIJ Int*., 51(2011), No. 10, p. 1601.

[10] Z.L. Zhao, H.Q. Tang, and Z.C. Guo, Effects of CaO on precipitation morphology of metallic iron in reduction of iron oxides under CO atmosphere, *J. Iron Steel Res.*, 20(2013), No. 7, p. 16.

[11] L. Guo, J.T. Gao, Y.W. Zhong, H. Gao, and Z.C. Guo, Phosphorus removal of high phosphorous oolitic iron ore with acid-leaching fluidized-reduction and melt-separation process, *ISIJ Int*., 55(2015), No. 9, p. 1806.

[12] H.Q. Tang, W.D. Liu, H.Y. Zhang, and Z.C. Guo, Effect of microwave treatment upon processing oolitic high phosphorus iron ore for phosphorus removal, *Metall. Mater. Trans. B*, 45(2014), No. 5, p. 1683.

[13] T. Hamano, S. Fukagai, and F. Tsukihashi, Reaction mechanism between solid CaO and FeO_x–CaO–SiO_2–P_2O_5 slag at 1573 K, *ISIJ Int.*, 46(2006), p. 490.

[14] S. Fukagai, T. Hamano, and F. Tsukihashi, Formation reaction of phosphate compound in multi phase flux at 1573 K, *ISIJ Int*., 47(2007), No. 1, p. 187.

[15] L.X. Zhao, Z.C. Guo, Z. Wang, and M.Y. Wang, Influences of super-gravity field on aluminum grain refining, *Metall. Mater. Trans. A*, 41(2010), No. 3, p. 670.

[16] L.X. Zhao, Z.C. Guo, Z. Wang, and M.Y. Wang, Removal of low-content impurities from Al by super-gravity, *Metall. Mater. Trans. B*, 41(2010), No. 3, p. 505.

[17] L. Guo, H. Gao, J.T. Yu, Z.L. Zhang, and Z.C. Guo, Influence of hydrogen concentration on Fe_2O_3 particle reduction in fluidized beds under constant drag force, *Int. J. Miner. Metall. Mater.*, 22(2015), No. 1, p. 12.